Assessing GNSS-based potential evapotranspiration: Comparison with empirical models and global datasets in the Los Angeles region

Saeed Ebrahimi *, Yazdan Amerian

Faculty of Geodesy and Geomatics Engineering, K. N. Toosi University of Technology, Tehran 1996715433, Iran
s.ebrahimi@email.kntu.ac.ir; amerian@kntu.ac.ir.

Keywords: PET, PWV, GNSS, GNSS-based method, Global gridded products, Traditional empirical methods.

Abstract
Potential evapotranspiration (PET) is a key component in the water exchange between the land surface and the atmosphere and plays a fundamental role in the hydrological cycle. While numerous methods approaches have been developed for estimating PET based on data inputs, evaluating the performance of new methods in comparison with common empirical methods is essential to achieve an optimal PET estimation method under data-limited conditions. In this study, precipitable water vapor (PWV) derived from Global Navigation Satellite Systems (GNSS) is used to estimate PET (GNSS-based PET). The GNSS-based PET is then evaluated along with two temperature-based methods (Hargreaves-Samani and Thornthwaite), two radiation-based methods (Priestley-Taylor and Makkink), and three global gridded PET products, including the ERA5-Land reanalysis model from the European Centre for Medium Range Weather Forecasts (ECMWF), the Global Land Evaporation Amsterdam Model (GLEAM version 4.2a), and the Global Land Data Assimilation System (GLDAS version 2.1). The Penman-Monteith method, endorsed by the Food and Agriculture Organization (FAO), was selected as the benchmark to evaluate the performance of all studied methods. Statistical evaluation results indicated that the GNSS-based method exhibited the highest agreement with the Penman-Monteith method compared to the other approaches. For this method, the root mean square error (RMSE) is 0.31 mm, the mean absolute error (MAE) is 0.27 mm, and the correlation coefficient (CC) is 0.97. These results demonstrate the superiority of the GNSS-based method in estimating PET.

1. Introduction

Evapotranspiration (ET) refers to the combined process of water evaporation from various surfaces and transpiration from plants, along with its transport into the atmosphere (Allen et al., 1998). Potential evapotranspiration (PET), as a physical process, represents the maximum amount of water that can be returned to the atmosphere under ideal conditions of soil moisture and vegetation cover (Thornthwaite, 1948). PET can also be introduced as an essential component of the water cycle that plays a central and extensive role in hydroclimatic studies. Changes in PET rate affect surface runoff, groundwater level, and water storage in the basin. When the PET rate increases, it can lead to reduced water for agricultural crops (McKenney and Rosenberg, 1993). Accurate PET estimates can provide useful information about the water requirements of plants (Fisher et al., 2011). PET is also applied in drought monitoring studies (Sheffield et al., 2012; Vicente-Serrano et al., 2010), agricultural water management (Anapalli et al., 2019), and environmental studies such as the urban heat island (QIU et al., 2013) and carbon dioxide (Chen et al., 2025). PET values are affected by meteorological factors such as temperature, solar radiation, humidity, and wind speed. Numerous empirical methods for estimating PET from various climatic variables have been developed over the past years, which include simple to complex methods depending on data requirements (Allen et al., 1998; McKenney and Rosenberg, 1993). The Penman-Monteith method (Allen et al., 1998) and the Thornthwaite method (Thornthwaite, 1948) as two common methods among multiple PET estimation approaches have been widely used in climatic studies. The Penman-Monteith method, as the most accurate and widely used method for estimating PET in different regions and climates, is approved by FAO. However, the complexity of the required inputs can lead to significant errors and extensive meteorological data are needed (Allen et al., 1998). In contrast, the Thornthwaite method only uses temperature but does not provide sufficient accuracy (Sheffield et al., 2012), and both methods are based on data measured at meteorological sites. The insufficient density and inappropriate distribution of meteorological stations worldwide and, secondly, the lack of complete climatic data in many meteorological stations create limitations for estimating accurate (Aschonitis et al., 2021). Therefore, examining newer methods for estimation optimal PET with fewer meteorological parameters along with reducing spatial limitations has attracted the attention of researchers. In recent years, Global Navigation Satellite Systems (GNSS), by providing accurate and continuous data, have been considered as a new source in atmospheric and hydrological studies such as three-dimensional estimation of wet refractivity (Haji-Aghajany, 2021), tropospheric delay prediction (Haji-Aghajany et al., 2024a), wet refractivity prediction (Haji-Aghajany et al., 2024b), advanced tropospheric tomography (Haji-Aghajany et al., 2025; Izanlou et al., 2024), flood prediction (Sorkhabi and Djamour, 2024), rainfall prediction (Yin et al., 2025), regional subsidence prediction (Tasan et al., 2023) and even urban temperature monitoring (Tasan et al., 2024), increasing the accuracy of the displacement fields (Maddahi et al., 2024), and ground water level monitoring (Haji-Aghajany et al., 2023). Water vapor, as one of the most important greenhouse gases and a key component in the hydrological cycle, has a significant effect on accurate PET estimation. GNSS technology, by providing precise atmospheric parameters, especially parameters such as Zenith Tropospheric Delay (ZTD), zenith wet delay (ZWD), makes it possible to obtain continuous water vapor with high temporal resolution under all weather conditions (Bevis et al., 1992). many studies have investigated the possibility of using GNSS-based PWV as an input variable in PET estimation. In this context, (MORI et al., 2007) presented a new approach for estimating PET based on

* Corresponding Author

PWV and land surface temperature in Japan. (Zhao et al., 2019), in a study in the Loess Plateau of China, modeled PET using PWV to calculate drought indices accurately, and later (Zhao et al., 2021) with an optimized method extended their previous model to the entire study area. (Ma et al., 2021) examined PET modeling methods using PWV across China. (Pipatsitee et al., 2023) in Thailand modeled PET from the Penman-Monteith method using PWV. Finally, the study of (Ebrahimi et al., 2025) in California showed that GNSS observations can play a decisive role in improving the accuracy of PET modeling and prediction using machine learning methods. Overall, despite the development of linear and nonlinear equations as well as artificial intelligence models in recent studies of PET modeling using GNSS products, no comprehensive investigation has been conducted to compare this novel approach with PET models that are widely used globally, with previous efforts focusing primarily on model development. The present study aims solely to compare the nonlinear GNSS-based algorithm developed in this research with traditional empirical PET models and global gridded PET products. More specifically, this study addresses the question of how the GNSS-based approach developed here ranks in terms of accuracy compared to other widely used global methods. For the GNSS-based PET modeling, the difference in PET between the Penman-Monteith and Thornthwaite methods is first calculated. The PET difference between the two methods is modeled using a multiple quadratic polynomial regression model. Independent variables include PWV obtained from GNSS observations, air temperature, as well as coordinate and time parameters. The modeled PET value is then added to the initial PET obtained from the Thornthwaite method. Subsequently, PET from traditional empirical methods is calculated using meteorological data, and PET from global gridded products is interpolated at the study site locations. For a comprehensive evaluation, all approaches studied are compared with the Penman-Monteith method.

2. Materials and Methods

2.1 Penman-Monteith Method

Considered the most accurate approach for estimating PET, the Penman-Monteith method incorporates all key climatic factors affecting evapotranspiration. It is widely recognized internationally as a benchmark for evaluating other empirical methods (Allen et al., 1998). The Penman-Monteith equation for calculating PET can be expressed as follows:

$$PET\_PM = \frac{0.408\Delta(R_n - G) + \gamma \frac{900}{T+273} u_2 (e_s - e_a)}{\Delta + \gamma(1 + 0.34\ u_2)} \quad (1)$$

where T is the mean air temperature $°C$, and u_2 is the mean wind speed at a height of two meters $(m.s^{-1})$. R_n is the net radiation and G is the soil heat flux, both with the same unit $(MJ.m^{-2}day^{-1})$. e_s is the Saturation vapor pressure and e_a is the actual vapor pressures, both with the same unit (kpa) . Δ is the slope of saturation vapor pressure curve, and γ is the psychrometric constant, both with the same unit $(kpa.°C^{-1})$.

2.2 Radiation-Based Methods

The estimation of PET relies on solar radiation as the main energy source driving evapotranspiration. Among the existing techniques, radiation-based methods have become common due to their physical relevance and relative simplicity(Xu and Singh, 2000). In addition to radiation variables, these methods also consider air temperature to provide a better representation of the surface energy balance. Although temperature appears in most formulations, these methods are classified as “radiation-based” to distinguish them from those that primarily depend on air temperature (Fisher et al., 2011).

2.2.1 Priestley-Taylor Method

Using net solar radiation, PET can be estimated through a simplified form of the (Penman, 1948), known as the Priestley-Taylor method (PRIESTLEY and TAYLOR, 1972).

$$PET\_PT = \alpha \frac{\Delta}{\Delta + \gamma} \frac{R_n - G}{\lambda} \quad (2)$$

Where λ is the latent heat of vaporization with the unit $(MJ.kg^{-1})$, and α is the empirical Priestley-Taylor coefficient $(\alpha = 1.26)$. Other parameters are defined in Equation (1).

2.2.2 Makkink Method

Designed for limited climatic data, Makkink method relies on solar radiation and temperature(Makkink, 1957).It represents a simplified modification of the (Penman, 1948), enabling PET estimation in data-scarce environments.

$$PET - MAK = c \frac{\Delta}{\Delta + \gamma} \frac{R_s}{\lambda} \quad (3)$$

Where R_s is the solar radiation $(MJ.m^{-2}day^{-1})$ and c denotes the empirical Makkink coefficient $(c = 0.61)$. Other parameters are defined in Equation (1).

2.3 Temperature-Based Methods

When solar radiation, relative humidity, or wind speed data are unavailable, temperature-based methods are employed. These methods estimate PET using only air temperature as the input parameter (Xu and Singh, 2001).

2.3.1 Hargreaves-Samani Method

PET can be estimated using daily air temperature and the difference between maximum and minimum temperatures, as in the Hargreaves-Samani equation (H. Hargreaves and A. Samani, 1985). According to (Allen et al., 1998), this approach can serve as a practical alternative to the Penman-Monteith equation when only air temperature data are available.

$$PET\_HS = 0.0023(T_{max} - T_{min})^{0.5}(T_{mean} + 17.8)R_a \quad (4)$$

Where T_{max} , T_{min} , T_{mean} are the maximum, minimum, and mean air temperatures $°C$, respectively, and R_a is the extraterrestrial radiation with the unit $(MJ.m^{-2}day^{-1})$.

2.3.2 Thornthwaite Method

The Thornthwaite method is a simple empirical equation that estimates PET using only mean air temperature as an input parameter (Thornthwaite, 1948).

$$PET\_TH = 16K(10\frac{T_m}{I})^a \quad (5)$$

Where T_m is the mean air temperature $°C$, I is the annual heat index, and a is a constant coefficient that is a function of the annual heat index. K is introduced as a correction coefficient, which is a function of latitude and solar declination.

2.4 GNSS-Based Method

2.4.1 Relationships Governing the Estimation of PWV from GNSS Observations

One of the major atmospheric effects on signals transmitted from remote sensing satellites such as GNSS and SAR, is the delay caused by the passage of these signals through the troposphere (Haji-Aghajany and Amerian, 2020; Mendes, 1998), which is measured in the vertical direction and is referred to as the ZTD. The ZTD consists of two separate components: the hydrostatic component (ZHD), which depends on the composition of dry atmospheric gases and surface pressure and can usually be modeled with good accuracy, and the wet component (ZWD), which represents the effect of atmospheric water vapor and is more variable in both time and space (Bevis et al., 1992). To obtain ZTD values, GNSS observations are processed using the Bernese software (Abdallah, 2016), based on the precise point positioning (PPP) method. The ZHD can be derived from the Saastamoinen empirical dry model, which is one of the most accurate global prediction models (Saastamoinen, 1972).

$$ZHD = \frac{0.002277P_s}{(1-0.0026\cos 2\varphi_s - 0.00000028h_s)} \quad (6)$$

Where P_s is the surface pressure at the station (hpa), φ_s is the station latitude, and h_s is the station height (m).

The value of ZWD is obtained by subtracting the value of ZHD from the value of ZTD. The ZWD is directly related to atmospheric water vapor (Bevis et al., 1992), and the PWV is calculated from ZWD using the following relation:

$$PWV = \Pi \cdot ZWD \quad (7)$$

In relation (7), the parameter Π depends on the weighted mean temperature T_m, as follows:

$$\Pi = [10^{-6}(\frac{k_3}{T_m} + k_2^{'})\rho_w.R_v]^{-1} \quad (8)$$

Where R_v is the universal specific gas constant for water vapor $(R_v = 461.50\ J.kg^{-1}.K^{-1})$, $k_2^{'}$ is an empirical physical constant $(k_2^{'} = 16.48\ K.hPa^{-1})$, k_3 is also an empirical physical constant $(k_3 = 3.776 \times 10^5\ K^2.hPa^{-1})$, and ρ_w is the density of liquid water $(\rho_w = 1000\ kg.m^{-3})$.

The weighted mean temperature is calculated using the following equation (Bevis et al., 1992).

$$T_m = \frac{\int_{h_s}^{\infty}\frac{e}{T}dh}{\int_{h_s}^{\infty}\frac{e}{T^2}dh} \approx \frac{\sum_{i=1}^{n}\left(\frac{e_i}{T_i}\right)(h_i - h_{i-1})}{\sum_{i=1}^{n}\left(\frac{e_i}{T_i^2}\right)(h_i - h_{i-1})} \quad (9)$$

Where e and T represent the actual water vapor pressure (hpa) and temperature $(°K)$ at each pressure level. Respectively, h represents the altitude of each pressure level.

2.4.2 PET Modeling Based on Regression Analysis

The Thornthwaite method, because it does not consider climatic parameters such as solar radiation, wind speed, and air humidity, tends to underestimate PET. In contrast, the Penman-Monteith method, by comprehensively accounting for climatic conditions, provides higher accuracy in PET estimation. In this section, the difference between the results of the Penman-Monteith and Thornthwaite equations (DPET) is being modeled with the aim of reducing the systematic errors of the Thornthwaite method and improving model performance.

$$DPET = PET\_PM - PET\_TH \quad (10)$$

The modeling of $DPET$ was considered to produce an optimal estimator model as a function of variables, temperature, time parameter, and coordinate parameters.

$$DPET = \mathrm{F}(pwv, T, t, \varphi, \lambda, h) \quad (11)$$

where pwv represents the mean precipitable water vapor, T denotes the mean air temperature, t is the time parameter, φ, λ and h correspond to latitude, longitude, and elevation, respectively.

In this section, with the aim of modeling the function, regression analysis was employed to identify and determine the relationship between the dependent variable and the independent variables. Accordingly, the model parameters were structured to achieve the best fit based on a multiple quadratic polynomial regression model, as follows:

$$\underbrace{\begin{bmatrix} DPET_1 \\ DPET_2 \\ \vdots \\ DPET_r \end{bmatrix}}_{L} = \underbrace{\begin{bmatrix} 1 & pwv & T & t & t^2 & \varphi & \lambda & h & \varphi\lambda & \varphi h & \lambda h & \varphi^2 & \lambda^2 & h^2 \end{bmatrix}}_{A} \times \underbrace{\begin{bmatrix} a_0 \\ a_1 \\ \vdots \\ a_u \end{bmatrix}}_{X} \quad (12)$$

Subsequently, the least squares adjustment method was applied to optimize the model coefficients in the region.

$$X_{u\times 1} = (A_{u\times r}{}^{T} A_{r\times u})^{-1} A_{u\times r}{}^{T} L_{r\times 1} \quad (13)$$

where $r = s \times m$, s is the number of stations, m is the number of samples within the modeling period, u is the number of unknown coefficients.

Finally, to obtain PET from the GNSS-based method, the *DPET* derived from modeling is added to the initial PET obtained from the Thornthwaite method.

$$PET\_GB = PET\_TH + DPET \quad (14)$$

3. Study Area and Data

3.1 Study Area and Time Period

The study area is bounded between latitudes 33° to 35°N and longitudes 118°W to 120°W, covering the Los Angeles Basin in the southwestern part of California, USA. This region was selected due to its climatic diversity and the availability of both meteorological and GNSS stations. The study utilized a 24-month dataset spanning from 2021 to 2022. For modeling purposes, 80% of the data (approximately the first 20 months) was allocated to the training phase. The remaining 20% (the final four months of 2022: September, October, November, and December) was reserved exclusively for evaluating model performance during the prediction timeframe.

3.2 Meteorological and GNSS Data

In this study, data from 13 ground meteorological stations were used from the Western Regional Climate Center (WRCC) database. WRCC is one of the six Regional Climate Centers (RCC) in the United States, managed by the National Oceanic and Atmospheric Administration (NOAA), and provides climate services related to the western region of the United States. In addition, observations from 13 GNSS stations were used from the UNAVCO database. UNAVCO is a scientific and research institution that provides the required infrastructure for geodetic and Earth science studies. In total, 26 ground meteorological and GNSS stations were selected and used in this study, which are shown in Figure 1.

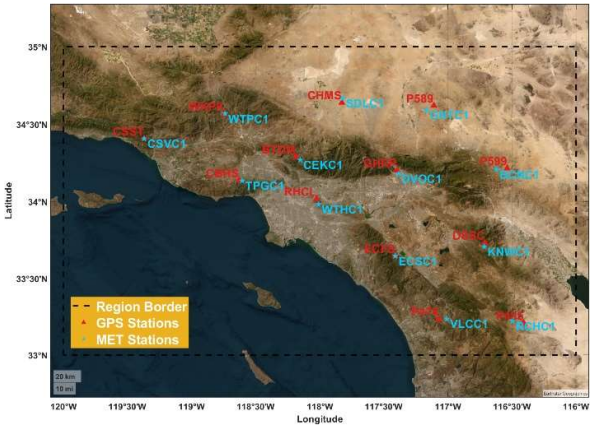

Figure 1. Distribution of the meteorological and GNSS stations in the study area

3.3 ERA5 Reanalysis Model (ECMWF)

The fifth generation of atmospheric reanalysis data (ERA5), developed by the European Centre for Medium-Range Weather Forecasts (ECMWF), provides a comprehensive set of meteorological parameters with high spatial and temporal resolution. Continuously updated since 1979, ERA5 offers global atmospheric variables on a 0.25° × 0.25° horizontal grid. Due to its high accuracy and global coverage, ERA5 products have been widely used in various fields, including GNSS-based meteorology. A notable advantage of ERA5 is its provision of hourly atmospheric variables across 37 pressure levels, making it an ideal tool for estimating precipitable water vapor (PWV) with high temporal resolution (Hersbach et al., 2020). In this study, ERA5 temperature and pressure data were employed to estimate PWV.

3.4 Global Gridded PET Products

3.4.1 ERA5-Land Model

ERA5-Land is a high-resolution reanalysis product developed by ECMWF, designed specifically for land applications. It provides hourly gridded atmospheric and land-surface data with a spatial resolution of approximately 0.1°× 0.1°, making it suitable for regional and local-scale climate, hydrological, and agricultural studies (Muñoz-Sabater et al., 2021). In this dataset, potential evapotranspiration (PET-ERA5Land) is computed using the Penman-Monteith equation (Singer et al., 2021).

3.4.2 GLEAM 4.2a Model

The Global Land Evaporation Amsterdam Model (GLEAM) represents one of the earliest approaches for estimating global evapotranspiration based on satellite observations. GLEAM datasets are updated at least annually and are freely and widely accessible. In this study, version 4.2a of GLEAM (PET-GLEAM4.2a) was employed, which offers improved spatial resolution (0.1°× 0.1° instead of 0.25°× 0.25°) and an extended temporal record (1980-2023) compared to earlier releases. Unlike previous versions, which used the Priestley-Taylor method, GLEAM 4.2a estimates evapotranspiration using the more accurate Penman (1948) formulation (Miralles et al., 2025).

3.4.3 GLDAS 2.1 Model

The Global Land Data Assimilation System (GLDAS) is an advanced global modeling framework jointly developed by NASA, the Goddard Space Flight Center (GSFC), NOAA, and the National Centers for Environmental Prediction (NCEP). Designed to generate optimal land surface states and fluxes, GLDAS integrates satellite and ground-based observations through advanced data assimilation techniques and land surface models such as Mosaic, Noah, CLM, and VIC (Rodell et al., 2004). PET in GLDAS is computed using a modified Penman–Monteith equation within the Noah land surface model, where land-surface parameters are specifically incorporated for PET estimation (Xu et al., 2024). In this study, PET data from the Noah model GLDAS version 2.1 (PET-GLDAS2.1) with a spatial resolution of 0.25°× 0.25° were used.

4. Results Analysis

4.1 Statistical Criteria

To evaluate the accuracy of the methods employed for estimating PET, commonly used statistical indices, including Root Mean Square Error (RMSE), Mean Absolute Error (MAE), and the Pearson Correlation Coefficient (CC), were applied.

This contribution has been peer-reviewed. The double-blind peer-review was conducted on the basis of the full paper.
https://doi.org/10.5194/isprs-annals-X-4-W8-2025-211-2026 | © Author(s) 2026. CC BY 4.0 License.

$$RMSE = \sqrt{\frac{1}{k}\sum_{i=1}^{k}\left(PET_{PM}^{i} - PET_{GB}^{i}\right)^{2}} \quad (15)$$

$$MAE = \frac{1}{k}\sum_{i=1}^{k}\left|PET_{PM}^{i} - PET_{GB}^{i}\right| \quad (16)$$

$$CC = \frac{\sum_{i=1}^{k}\left(PET_{PM}^{i} - \overline{PET}_{PM}\right)\left(PET_{GB}^{i} - \overline{PET}_{GB}\right)}{\sqrt{\left[\sum_{i=1}^{k}\left(PET_{PM}^{i} - \overline{PET}_{PM}\right)^{2}\sum_{i=1}^{k}\left(PET_{GB}^{i} - \overline{PET}_{GB}\right)^{2}\right]}} \quad (17)$$

Where PET_{PM} is the reference values obtained from the Penman-Monteith method, PET_{GB} is the predicted values derived from the GNSS-based method, $\overline{PET}_{PM}$ is the mean of the reference values, $\overline{PET}_{GB}$ is the mean of the predicted values, and k is the number of samples.

Lower RMSE and MAE values represent higher model accuracy, while a correlation coefficient closer to +1 indicates a stronger linear agreement between modeled and reference data.

4.2 Statistical Evaluation of Results

In this section, the PET results obtained from the GNSS-based method, radiation-based methods, temperature-based methods, and interpolated global gridded PET products are evaluated using statistical error indices including RMSE, MAE, and r. Figure 2 presents the results of RMSE (a), MAE (b), and CC (c) for the studied methods compared with the reference Penman-Monteith method in the region. The Penman-Monteith method accounts for all climatic factors influencing the PET process and provides highly accurate results. In contrast, traditional empirical approaches, including radiation-based and temperature-based methods, suffer from deficiencies in input data and therefore exhibit limited accuracy. Among these, the Thornthwaite method is the simplest, relying only on mean temperature, which leads to underestimation of PET. According to Figure 2 (a) and (b), Thornthwaite records the weakest results among all models in terms of RMSE and MAE. On the other hand, the most accurate empirical method after Penman-Monteith is the Hargreaves-Samani method, which requires maximum, minimum, and mean air temperature, and yields more accurate results compared to other empirical methods. Among the radiation-based methods, Priestley-Taylor demonstrates higher accuracy than Makkink, with both performing better than Thornthwaite. Regarding global gridded PET products, since the ERA5-Land dataset is derived using the Penman-Monteith method, its results are more accurate than those of GLEAM 4.2a and GLDAS 2.1.

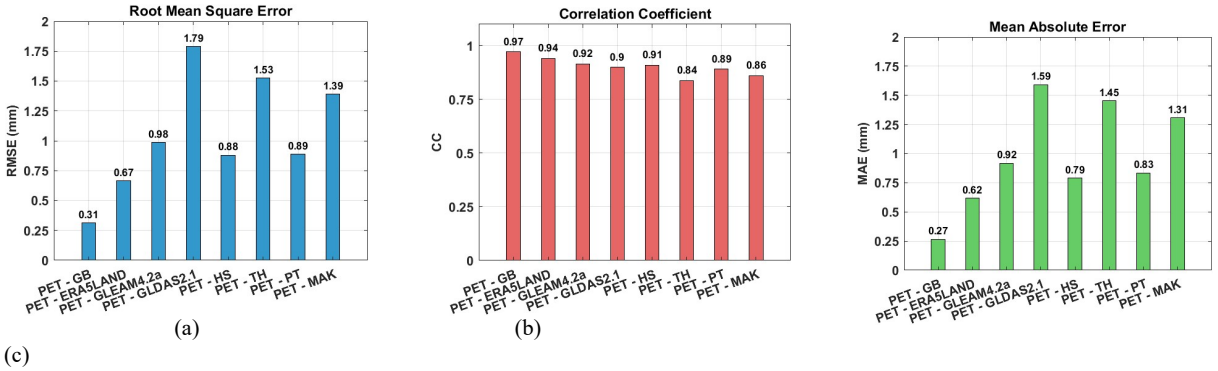

(a) (b) (c)

Figure 2. RMSE, MAE and Correlation Coefficient values obtained from PET estimation approaches (empirical methods, global gridded Products, and the GNSS-based method) during the prediction timeframe

GLEAM 4.2a applies the Penman (1948) approach for PET estimation and provides better accuracy than GLDAS 2.1. However, GLDAS 2.1, which employs a modified Penman-Monteith formulation, tends to overestimate PET. As clearly shown in Figure 2 (a-c), the statistical error indices highlight the superior performance of the GNSS-based method in the region The evaluation results, including RMSE is 0.31, MAE is 0.27, and CC is 0.97, confirm the high precision and reliability of this method, while other methods demonstrate lower accuracy.
Overall, the findings demonstrate that based on the RMSE and MAE criteria, the highest accuracy compared to the Penman-Monteith method corresponds respectively to the following approaches: 1. PET_GB, 2. PET_ERA5LAND, 3. PET_HS, 4. PET_PT, 5. PET_GLEAM4.2a, 6. PET_MAK, 7. PET_TH, and 8. PET_GLDAS2.1.

In terms of the correlation coefficient, the strongest correlation with the Penman–Monteith method is achieved respectively by: 1. PET_GB, 2. PET_ERA5LAND, 3. PET_GLEAM4.2a, 4. PET_HS, 5. PET_GLDAS2.1, 6. PET_PT, 7. PET_MAK, and 8. PET_TH.

4.3 Numerical Evaluation of the Results

In this section, the numerical results of GNSS-based PET modeling are discussed and compared with PET derived from traditional empirical methods and global gridded PET products. The mean PET values obtained during the prediction timeframe from the investigated approaches are presented in Figure 3, These numerical results indicate that the GNSS-based method has the highest consistency with the Penman-Monteith method.

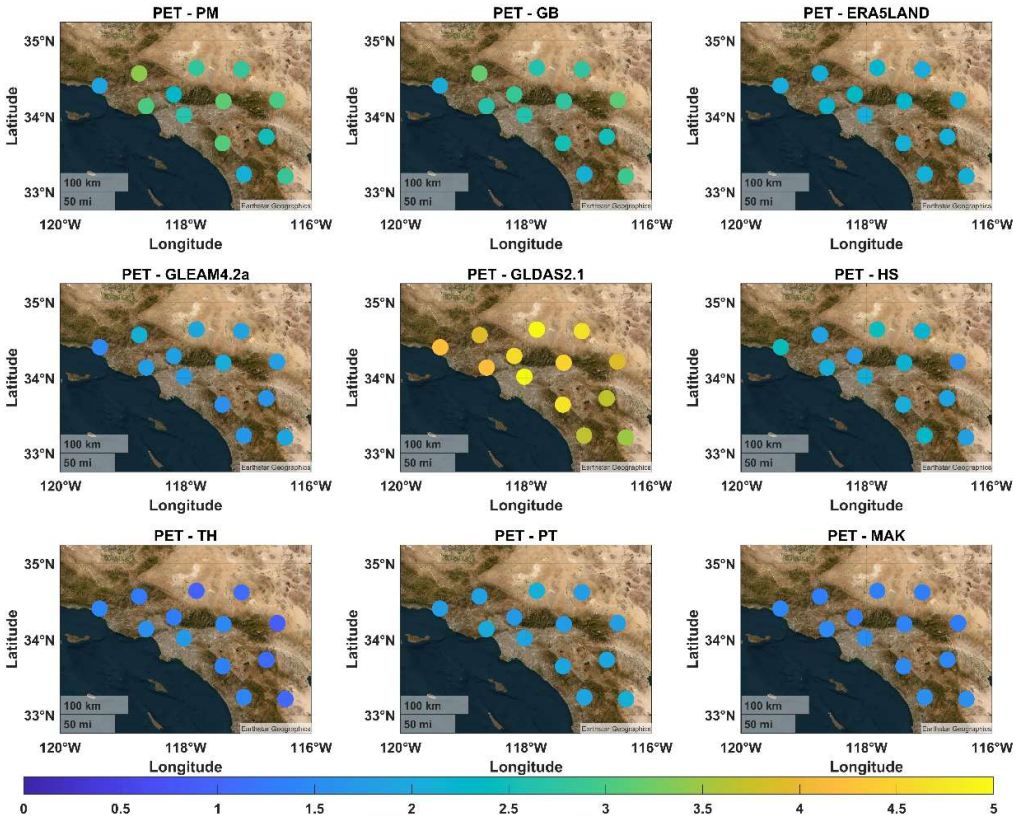

Figure 3. PET mean values (mm) derived from (empirical methods, global gridded Products, and GNSS-based method)

Figure 4, illustrates the cumulative PET for the entire prediction period in the form of a bar chart. The cumulative PET obtained from the GNSS-based method was 239.7 mm, showing a negligible difference of 6.6 mm compared with the 246.3 mm obtained from the Penman-Monteith method.

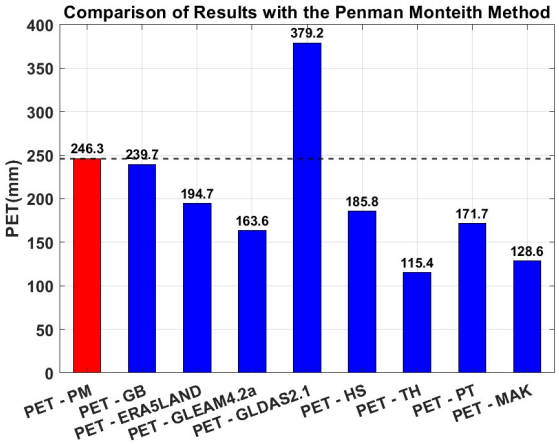

Figure 4. Total PET values derived from (empirical methods, global gridded Products, and GNSS-based method)

Table 1, shows the differences in PET values between all approaches and the Penman-Monteith method. According to Table 1, the smallest differences relative to the Penman-Monteith method were observed in the following order: 1. PET_GB, 2. PET_ERA5LAND, 3. PET_HS, 4. PET_PT, 5. PET_GLEAM4.2a, 6. PET_MAK, 7. PET_TH, 8. PET_GLDAS2.1. Collectively, these results clearly demonstrate the superiority of the GNSS-based method in providing accurate PET estimates.

Methods	Difference(mm)
PET_GB	**6.6**
PET_ERA5LAND	**51.6**
PET_GLEAM4.2a	**82.7**
PET_GLDAS2.1	**132.9**
PET_HS	**60.5**
PET_TH	**130.9**
PET_PT	**74.6**
PET_MAK	**117.7**

Table 1. Differences in Total PET values between Penman-Monteith method and (empirical methods, global gridded Products, and GNSS-based method)

5. Conclusion

This study evaluated the performance of GNSS-based PET estimation method that used only temperature and PWV data, comparing it with empirical temperature-based and radiation-based methods and global PET products. Results showed that the GNSS-based approach had the best agreement with the Penman-Monteith estimates, with the smallest mean difference of 6.6 mm. However, the findings should be interpreted with caution. The analysis was limited to a specific climatic region and time period. Moreover, the performance of this method may vary under extreme weather conditions or in regions with sparse GNSS coverage. Although the proposed approach demonstrates strong potential, it still relies on temperature and PWV data from a dense

GNSS network-an infrastructure that is often unavailable in developing countries. Therefore, its practical applicability in less-developed regions remains limited. Despite these limitations, the advancement of GNSS technology has enabled the retrieval of PWV data with high spatial and temporal accuracy. This capability makes the GNSS-based PET estimation a promising tool for improving PET monitoring networks. Expanding the integration of GNSS observations with existing meteorological networks could ultimately contribute to the development of a global PET monitoring system.

Data availability statement

The data that support the findings of this study are available upon request from the authors.

Reference

Abdallah, A., 2016. Short Toturial for Bernese GNSS Software V. 5.2. pp. 119–128.

Allen, R., Pereira, L., Raes, D., Smith, M., 1998. FAO Irrigation and drainage paper No. 56. Rome Food Agric. Organ. U. N. 56, 26–40.

Anapalli, S.S., Fisher, D.K., Reddy, K.N., Rajan, N., Pinnamaneni, S.R., 2019. Modeling evapotranspiration for irrigation water management in a humid climate. Agric. Water Manag. 225, 105731. https://doi.org/10.1016/j.agwat.2019.105731

Aschonitis, V., Touloumidis, D., Ten Veldhuis, M.-C., Coenders-Gerrits, M., 2021. Correcting Thornthwaite potential evapotranspiration using a global grid of local coefficients to support temperature-based estimations of reference evapotranspiration and aridity indices. https://doi.org/10.5194/essd-2021-115

Bevis, M., Businger, S., Herring, T., Rocken, C., Anthes, R., Ware, R., 1992. GPS Meteorology: Remote Sensing of Atmospheric Water Vapor Using the Global Positioning System. J. Geophys. Res. 97. https://doi.org/10.1029/92JD01517

Bruno, D., Ryan, G., Kaplan, C., Slemmer, J., 2000. Climate of Los Angeles, California. NOAA technical memorandum NWS WR ; 261.

Chen, J., Tang, Z., Kang, X., He, N., Li, M., 2025. Rise in wetland carbon uptake linked to increased potential evapotranspiration. Environ. Res. 279, 121778. https://doi.org/10.1016/j.envres.2025.121778

Ebrahimi, A.S., Haji-Aghajany, B.S., Amerian, C.Y., Tasan, D.M., 2025. EvapoDeep: A Dual Deep Learning Framework utilizing GNSS data for Evapotranspiration Modeling and Predictive Analysis. IEEE J. Sel. Top. Appl. Earth Obs. Remote Sens.

Fisher, J.B., Whittaker, R.J., Malhi, Y., 2011. ET come home: potential evapotranspiration in geographical ecology. Glob. Ecol. Biogeogr. 20, 1–18. https://doi.org/10.1111/j.1466-8238.2010.00578.x

H. Hargreaves, G., A. Samani, Z., 1985. Reference Crop Evapotranspiration from Temperature. Appl. Eng. Agric. 1, 96–99. https://doi.org/10.13031/2013.26773

Haji-Aghajany, S., 2021. Function-based troposphere water vapor tomography using GNSS observations. https://doi.org/10.13140/RG.2.2.21213.08162/2

Haji-Aghajany, S., Amerian, Y., 2020. Assessment of InSAR tropospheric signal correction methods. J. Appl. Remote Sens. 14, 13. https://doi.org/10.1117/1.JRS.14.044503

Haji-Aghajany, S., Amerian, Y., Amiri-Simkooei, A., 2023. Impact of Climate Change Parameters on Groundwater Level: Implications for Two Subsidence Regions in Iran Using Geodetic Observations and Artificial Neural Networks (ANN). Remote Sens. 15, 1555. https://doi.org/10.3390/rs15061555

Haji-Aghajany, S., Izanlou, S., Tasan, M., Rohm, W., Kryza, M., 2025. High-resolution GNSS troposphere tomography through explainable deep learning-based downscaling framework. Satell. Navig. 6. https://doi.org/10.1186/s43020-025-00177-6

Haji-Aghajany, S., Rohm, W., Hadas, T., Bosy, J., 2024a. Machine learning-based tropospheric delay prediction for real-time precise point positioning under extreme weather conditions. GPS Solut. 29, 36. https://doi.org/10.1007/s10291-024-01782-9

Haji-Aghajany, S., Rohm, W., Kryza, M., Smolak, K., 2024b. Machine Learning-Based Wet Refractivity Prediction Through GNSS Troposphere Tomography for Ensemble Troposphere Conditions Forecasting. IEEE Trans. Geosci. Remote Sens. https://doi.org/10.1109/TGRS.2024.3417487

Hersbach, H., Bell, B., Berrisford, P., Hirahara, S., Horányi, A., Muñoz-Sabater, J., Nicolas, J., Peubey, C., Radu, R., Schepers, D., Simmons, A., Soci, C., Abdalla, S., Abellan, X., Balsamo, G., Bechtold, P., Biavati, G., Bidlot, J., Bonavita, M., De Chiara, G., Dahlgren, P., Dee, D., Diamantakis, M., Dragani, R., Flemming, J., Forbes, R., Fuentes, M., Geer, A., Haimberger, L., Healy, S., Hogan, R.J., Hólm, E., Janisková, M., Keeley, S., Laloyaux, P., Lopez, P., Lupu, C., Radnoti, G., de Rosnay, P., Rozum, I., Vamborg, F., Villaume, S., Thépaut, J.-N., 2020. The ERA5 global reanalysis. Q. J. R. Meteorol. Soc. 146, 1999–2049. https://doi.org/10.1002/qj.3803

Izanlou, S., Haji-Aghajany, S., Amerian, Y., 2024. Enhanced Troposphere Tomography: Integration of GNSS and Remote Sensing Data With Optimal Vertical Constraints. IEEE J. Sel. Top. Appl. Earth Obs. Remote Sens. PP, 1–16. https://doi.org/10.1109/JSTARS.2024.3354884

Ma, X., Zhao, Q., Yao, Y., Yao, W., 2021. A novel method of retrieving potential ET in China. J. Hydrol. 598, 126271. https://doi.org/10.1016/j.jhydrol.2021.126271

Maddahi, S., Tasan, M., Haji-Aghajany, S., 2024. Enhancing InSAR accuracy: Unveiling more accurate displacement fields through 3-D troposphere tomography. J. Atmospheric Sol.-Terr. Phys. 256, 106207. https://doi.org/10.1016/j.jastp.2024.106207

Makkink, G.F., 1957. Testing the Penman formula by means of lysimeters. J. Inst. Water Eng. 11, 277–288.

McKenney, M.S., Rosenberg, N.J., 1993. Sensitivity of some potential evapotranspiration estimation methods to climate change. Agric. For. Meteorol. 64, 81–110. https://doi.org/10.1016/0168-1923(93)90095-Y

Mendes, V., 1998. Modeling the Neutral Atmosphere Propagation Delay in Radiometric Space Techniques.

Miralles, D.G., Bonte, O., Koppa, A., Baez-Villanueva, O.M., Tronquo, E., Zhong, F., Beck, H.E., Hulsman, P., Dorigo, W., Verhoest, N.E.C., Haghdoost, S., 2025. GLEAM4: global land evaporation and soil moisture dataset at 0.1° resolution from 1980 to near present. Sci. Data 12, 416. https://doi.org/10.1038/s41597-025-04610-y

MORI, M., HIRAMATSU, K., HARADA, M., 2007. Estimating Daily Potential Evapotranspiration using the Relation between GPS-derived Precipitable Water Vapor and Surface Temperature. Trans. Jpn. Soc. Irrig. Drain. Rural Eng. 2007, 347-352,a1. https://doi.org/10.11408/jsidre2007.2007.347

Muñoz-Sabater, J., Dutra, E., Agustí-Panareda, A., Albergel, C., Arduini, G., Balsamo, G., Boussetta, S., Choulga, M., Harrigan, S., Hersbach, H., Martens, B., Miralles, D.G., Piles, M., Rodríguez-Fernández, N.J., Zsoter, E., Buontempo, C., Thépaut, J.-N., 2021. ERA5-Land: a state-of-the-art global reanalysis dataset for land applications. Earth Syst Sci Data 13, 4349–4383. https://doi.org/10.5194/essd-13-4349-2021

Penman, H.L., 1948. Natural Evaporation from Open Water, Bare Soil and Grass. Proc. R. Soc. Lond. Ser. A 193, 120–145. https://doi.org/10.1098/rspa.1948.0037

Pipatsitee, P., Ninsawat, S., Tripathi, N.K., Shanmugam, M., Chitsutti, P., 2023. Estimating daily potential evapotranspiration using GNSS-based precipitable water vapor. Heliyon 9, e17747. https://doi.org/10.1016/j.heliyon.2023.e17747

PRIESTLEY, C.H.B., TAYLOR, R.J., 1972. On the Assessment of Surface Heat Flux and Evaporation Using Large-Scale Parameters. Mon. Weather Rev. 100, 81–92. https://doi.org/10.1175/1520-0493(1972)100%253C0081:OTAOSH%253E2.3.CO;2

QIU, G., LI, H., ZHANG, Q., CHEN, W., LIANG, X., LI, X., 2013. Effects of Evapotranspiration on Mitigation of Urban Temperature by Vegetation and Urban Agriculture. J. Integr. Agric. 12, 1307–1315. https://doi.org/10.1016/S2095-3119(13)60543-2

Rodell, M., Houser, P.R., Jambor, U.E.A., Gottschalck, J., Mitchell, K., Meng, C.-J., Arsenault, K., Cosgrove, B., Radakovich, J., Bosilovich, M., 2004. The global land data assimilation system. Bull. Am. Meteorol. Soc. 85, 381–394.

Saastamoinen, J., 1972. Contributions to the theory of atmospheric refraction. Bull. Géod. 1946-1975 105, 279–298. https://doi.org/10.1007/BF02521844

Sheffield, J., Wood, E., Roderick, M., 2012. Little Change in Global Drought over the Past 60 Years. Nature 491, 435–438. https://doi.org/10.1038/nature11575

Singer, M.B., Asfaw, D.T., Rosolem, R., Cuthbert, M.O., Miralles, D.G., MacLeod, D., Quichimbo, E.A., Michaelides, K., 2021. Hourly potential evapotranspiration at 0.1° resolution for the global land surface from 1981-present. Sci. Data 8, 224. https://doi.org/10.1038/s41597-021-01003-9

Sorkhabi, O.M., Djamour, Y., 2024. 4D modeling of precipitable water vapor to assess flood forecasting by using GPS signals. Nat. Hazards 120, 181–195. https://doi.org/10.1007/s11069-023-06185-6

Tasan, M., Ghorbaninasab, Z., Haji-Aghajany, S., Ghiasvand, A., 2023. Leveraging GNSS tropospheric products for machine learning-based land subsidence prediction. Earth Sci. Inform. 16. https://doi.org/10.1007/s12145-023-01143-z

Tasan, M., Voosoghi, B., Haji-Aghajany, S., Khalili, M.A., Di Martire, D., 2024. InSAR and GNSS data fusion for improved urban heat island estimation using local climate zone classification. Int. J. Appl. Earth Obs. Geoinformation 130, 103906. https://doi.org/10.1016/j.jag.2024.103906

Thornthwaite, C.W., 1948. An Approach toward a Rational Classification of Climate. Geogr. Rev. 38, 55–94. https://doi.org/10.2307/210739

Vicente-Serrano, S., Beguería, S., López-Moreno, J.I., 2010. A Multiscalar Drought Index Sensitive to Global Warming: The Standardized Precipitation Evapotranspiration Index. J. Clim. 23, 1696–1718. https://doi.org/10.1175/2009JCLI2909.1

Xu, C., Wang, W., Hu, Y., Liu, Y., 2024. Evaluation of ERA5, ERA5-Land, GLDAS-2.1, and GLEAM potential evapotranspiration data over mainland China. J. Hydrol. Reg. Stud. 51, 101651. https://doi.org/10.1016/j.ejrh.2023.101651

Xu, C.-Y., Singh, V.P., 2001. Evaluation and generalization of temperature-based methods for calculating evaporation. Hydrol. Process. 15, 305–319. https://doi.org/10.1002/hyp.119

Xu, C.-Y., Singh, V.P., 2000. Evaluation and generalization of radiation-based methods for calculating evaporation. Hydrol. Process. 14, 339–349. https://doi.org/10.1002/(SICI)1099-1085(20000215)14:2%253C339::AID-HYP928%253E3.0.CO;2-O

Yin, W., Zhou, C., Tian, Y., Qiu, H., Zhang, W., Chen, H., Liu, P., Zhao, Q., Kong, J., Yao, Y., 2025. Accurate Rainfall Prediction Using GNSS PWV Based on Pre-Trained Transformer Model. Remote Sens. 17. https://doi.org/10.3390/rs17122023

Zhao, Q., Ma, X., Yao, W., Liu, Y., Du, Z., Yang, P., Yao, Y., 2019. Improved Drought Monitoring Index Using GNSS-Derived Precipitable Water Vapor over the Loess Plateau Area. Sensors 19, 5566. https://doi.org/10.3390/s19245566

Zhao, Q., Sun, T., Zhang, T., He, L., Zhang, Z., Shen, Z., Si, X., 2021. High-Precision Potential Evapotranspiration Model Using GNSS Observation. Remote Sens. 13, 4848. https://doi.org/10.3390/rs13234848